Chapter 3

Materials and Methods

3. Materials and methods

3.1. Materials

This section provides information on the resources (microorganisms, apparatus, chemicals, and media) employed in the current investigation.

3.1.1. Microorganism

The *S. zooepidemicus* MTCC 3523 bacterial strain was acquired from the Microbial Type Culture Collection and Gene Bank (IMTECH), Chandigarh, India, in ampoules as a freeze-dried culture. After a 24-hour incubation period at 37 ºC, the strains were sustained by weekly transfers onto complex media (Amado et al., 2017) and reposited at 4 ºC.

3.1.2. Equipment

Autoclave (Khera Instruments, India) sterilizes the media before inoculation and the infected or fermented material before disposal.

Distilled Water plant (Infusil, India): It was used as a water supply for preparing media and conducting other experiments.

Digital weighing balance (Danwer Scales): weighed compounds (g level).

Cold centrifuge (Remi C 24 Plus, India): separates the insoluble components from the solution.

Hot air oven (Ikon instruments): used to dry glass objects.

Orbital Rotary Shaker Incubator (Remi CIS 24 plus, India): used to maintain a steady temperature for the growth of microbes.

Laminar air flow cabinet (Ikon instruments): to be utilized during aseptic inoculation.

Fridge (Whirlpool, India), Deep Fridge (Blue Star): For storing heat-sensitive substances and cultural preservation.

Heater (Bajaj, India): Used for heating purposes.

Magnetic stirrer (Remi, India): Used for mixing chemicals.

pH meter (Toshcon Industries): Used for pH measurement.

Viscometer (Brookfield, India): For measuring the broth viscosity.

UV-Vis Spectrophotometer (Shimadzu, Japan): Used for routine optical measurements.

Water bath (National Scientific): Used for carrying out experiments at a constant temperature.

Bioreactor (BioEngineering KLF, India): It was utilized to produce hyaluronic acid at specified conditions.

Fourier Transform Infrared Spectrometer (Shimadzu, Japan): Used to identify the functional groups in the hyaluronic acid sample and standard.

High-Performance Liquid Chromatography (Waters Alliance, USA): It was used for quantitative analysis of hyaluronic acid.

Nuclear magnetic resonance (BRUKER BioSpin INTERNATIONAL AG): To study matter's physical, chemical, and biological properties.

Scanning Electron Microscope (Oxford Instruments Nanoanalysis): projects and scans a focused stream of electrons over the HA surface to create an image.

High-Resolution X-Ray Diffraction (RIGAKU Corporation): to provide chemical information for elemental and phase analyses.

Thermogravimetric Analysis (M/s Shimadzu (Asia Pacific) Pte Ltd): It was utilized for HA thermal characterization.

X500 QTOF Mass Spectrometer (SCIEX): used to perform the ESI-MS observations.

3.1.3. Chemicals and Reagents

The following is a list of every chemical utilized in various experimental research that was purchased from Merck, SRL, HiMedia, India, and Sigma Co., USA:

Glucose, yeast extract, tryptone, potassium dihydrogen phosphate, magnesium sulfate, dipotassium hydrogen phosphate, ammonium sulfate, the pancreatic digest of protein, sodium bicarbonate, sodium chloride, dipotassium phosphate, sodium hydroxide, hydrochloric acid, activated charcoal, agar, 3,5-dinitro-salicylic acid, sodium dodecyl sulfate, Cetyl trimethyl ammonium bromide, methanol, ethanol, propanol, potassium bromide, acetic acid, fructose, xylose, lactose, dextrose, maltose, molasses, corn powder, tapioca powder, hyaluronic acid (standard), silicon oil, hexadecyltrimethylammonium bromide, calcium chloride, amber lite XAD-7 resins, n-hexane, ethyl acetate, acetone, and acetonitrile were utilized.

3.2. Media

3.2.1. Revival medium for *Streptococcus zooepidemicus*

The medium's revival was performed in the growth medium of (per liter), glucose 20g, yeast extract 10g, Dipotassium hydrogen phosphate 2g, magnesium sulfate 1g, and sodium chloride 2g.

The strain *Streptococcus zooepidemicus* was grown aerobically in 50 ml flasks containing a growth medium. The culture was grown in an incubator shaker (REMI, INDIA) at 100 rpm and 37 °C for 24 hours, and the initial pH was maintained at 6.8 using 2 M HCl and 2 M NaOH.

3.2.2. Seed Culture: Todd Hewitt Broth Composition

After the revival of the culture, Todd Hewitt broth was minded with the assemblage of (per liter) pancreatic digest of protein 10g, tryptone 20g, glucose 2g, sodium bicarbonate 2g, sodium chloride 2g, Dipotassium phosphate 0.4g. The strain *Streptococcus zooepidemicus* was grown aerobically in 250 ml flasks containing a growth medium. The culture was grown in an incubator shaker (REMI, INDIA) at 100 rpm and 37 ºC for 12 hours, and the initial pH was maintained at 6.8 using 2 M HCl and 2 M NaOH.

3.2.3. Sterilization of the media

The autoclave sterilized the media for 20 minutes at 121 ºC or 15 psi.

3.3. Experimental setup for hyaluronic acid production

A 2.5 L working volume, 3.7 L bench-scale bioreactor (Bioengineering) was used to produce hyaluronic acid. The following are the significant features of the bench-scale bioreactor (bioengineering) system:

The impeller used in the 3.7 L fermenter for properly mixing nutrients was bottom-driven type, with a turbine of 2 mm thick. The number of impellers used in the fermenter was 2, with six blades in each impeller. A ring-type sparger with 12 holes of 78 mm diameter was

used for proper aeration. Four numbers of baffles of 14 mm width were used in the fermenter. The working volume of the fermenter was 2.5 L.

The controllers for all critical parameters, such as agitation speed, pH, dissolved oxygen, and temperature, were equipped in a bioreactor. A pre-installed software program for fermentation (BioSCADA, flexible software adaptable to user requirements) was used for online monitoring and control of the fermentation process. To adjust the dissolved oxygen concentration level of the fermentation broth before the inoculation at 100%, the air was used as the inlet gas at the fermentation temperature. A polarographic-type dissolved oxygen probe (Mettler-Toledo, Switzerland) with the replaceable membrane was used to analyze the dissolved oxygen concentration.

It is connected to a dissolved oxygen analyzer of the computer-controlled fermentation system. A sterilizable pH electrode (Mettler-Toledo, Switzerland) was used to measure the culture broth's pH value. For the 3.7 L fermentor system, the supplied air, exhaust pipes, and other parts were sterilized by autoclave. A steam-heated jacket sterilized the culture vessel and broth.

Batch fermentation occurred in a 2.5-liter bioengineering bioreactor with a 3.7-liter capacity (Figure 3.1). A 5% (v/v) inoculum was supplemented to the autoclaved media, and the bioreactor was run at 37˚C with pH maintained at 6.8 with the help of 2 M NaOH and 2 M HCl. The agitation speed was achieved using an impellor of 100 rpm. A 5 ml sample was periodically supervened from the bioreactor aseptically and examined for sugar, biomass, and hyaluronic acid concentrations.

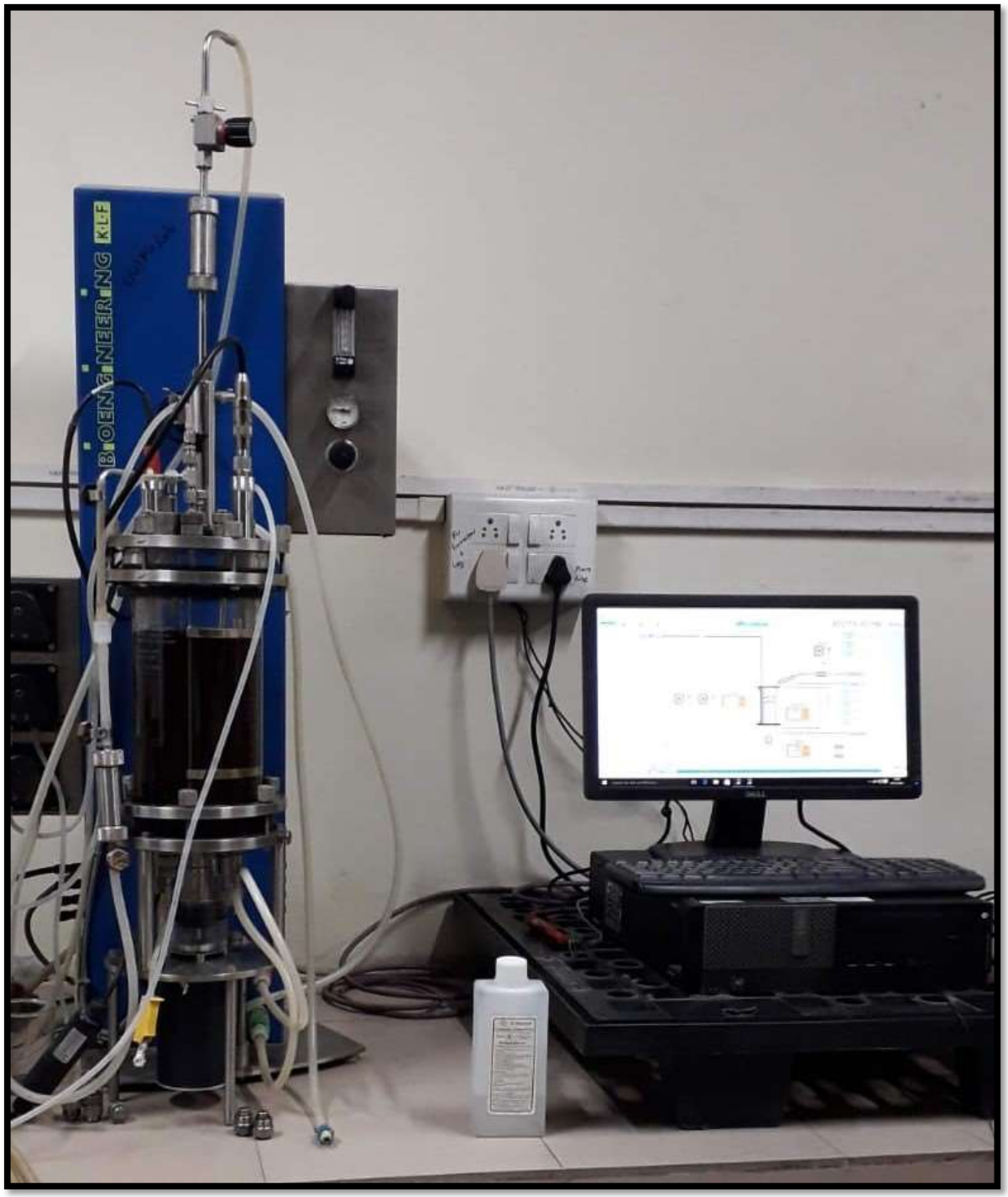

Figure 3.1. Experimental setup of bioreactor for production of hyaluronic acid.

3.4.Optimization of the medium for hyaluronic acid production

Batch fermentation took place in a 2.5-liter bioengineering bioreactor with a 3.7-liter capacity. A 5% (v/v) inoculum was supplemented to the autoclaved media, and the bioreactor was run at 37˚C with pH maintained at 6.8 with the help of 2 M NaOH and 2 M HCl.

The agitation speed was achieved using an impellor of 100 rpm. A 5 ml sample was periodically supervened from the bioreactor aseptically and examined for sugar, biomass, and hyaluronic acid concentrations.

3.4.1. Cell suspension preparation

S. zooepidemicus stock culture was inoculated onto complex medium plates, and cells were grown overnight at 37 ºC to create the inoculum suspension. Six round discs 0.90 cm in diameter were produced by punching the generated colonies with a sterile cork borer. Following that, the discs were placed in a sampling bottle that contained 50 ml of distilled water. To ensure that the cells were evenly disseminated, the sampling vial was vortexed for 3 minutes (Don & Shoparwe, 2010).

3.4.2. Inoculum preparation

A 50 mL sterile medium was used to incubate a 50 µL bacterial suspension (1.0×10^5 CFU/mL) for 12 hours at 37 ºC with agitation (100 rpm) and pH 7. The absorbance of the inoculum was measured to standardize it (OD_{600nm} ~ 0.4-0.6) and added to 200 mL of media to investigate flask culture studies.

3.4.3. One variable at a time optimization

During fermentation processes, optimization of the production medium and process conditions determines the microbe's growth and the product's quantity and quality (Stanbury et al., 2013). The upsurging of the HA production process was performed using the statistical tool. Parameters that directly affect the fermentation process were discovered and improved to obtain an increased production of HA.

The first factor directly influencing the process is the substrate used in the media. Different carbon substrates like fructose, xylose, lactose, dextrose, maltose, molasses, corn powder, and tapioca powder were examined for production, and the one with the most significant yield was selected for further optimization. The other factors, for instance, inoculum percentage, temperature, and agitation speed, were also optimized.

For determining the interrelationship between the preferred criterion and enhanced HA production, the response surface methodology based on the CCD was applied as a statistical technique (Himabindu et al., 2006; Saran et al., 2007). Utilizing the Minitab 16 program and analysis of variance (ANOVA), the data was examined to determine the synergy between the determinants and responses.

3.4.4. Optimization of fabrication of hyaluronic acid with RSM

Response surface methodology (RSM) is a compilation of statistical and mathematical tools extensively used for mounting, improving, and optimizing processes based on the fit of a polynomial equation to the experimental data. The most widespread application of RSM is to study several input variables' combined results and search for the best possible setting for a multivariable system. The main goal of the response surface is to efficiently hunt for the optimum values of the variables such that the response is maximized.

The input variables are called independent variables, i.e., they are subject to the control of the researchers. A combination of factors generating a specific optimum response can be recognized through factorial design and RSM.

In the present study, a Central Composite Design (CCD) based on RSM was used to analyze the effects of several parameters on the elution of hyaluronic acid. It has been a widely used statistical method based on multivariate nonlinear models for optimizing process variables. It also determines the appropriate experiments' regression model equations and operating conditions. All the experiments were performed in triplicates. In coded terms, the variables' lowest, central, and highest levels were -1, 0, and +1, respectively.

A total of 20 different combinations were chosen in random order according to a CCD configuration for three variables. The variables of the experiments were coded according to the following equation:

$$Coded\ value = \frac{Actual\ level \quad (Highe \quad level + Lower\ level)/2}{(High \quad level + Lower\ level)/2} \quad \text{Equation (1)}$$

The experimental data were analyzed by the response surface regression method to fit the following second-order polynomial equation:

$$Y = \beta_o + \Sigma\, \beta_i x_i + \Sigma\, \beta_{ii} x_i^2 + \Sigma\, \beta_{ij} x_i x_j \quad \text{Equation (2)}$$

Where Y is the predicted response, β_o is the offset term, β_i is the linear effect, β_{ii} is the square effect, and β_{ij} is the interaction effect. X_i is the i^{th} independent variable. The second-order polynomial coefficients were calculated using the Minitab software version 16.

The model's statistical analysis was performed as an analysis of variance (ANOVA). This analysis included Fisher's F-test (Overall model significance), its associated probability p(F), correlation coefficient R, and determination coefficient $R^{2,}$ which measures the goodness of

fit of a regression model. It also includes the Student's t-value for the estimated coefficients and the associated probabilities p(t). For each variable, the quadratic models were represented as surface plots.

The optimal combinations were determined from the surface plots. The current study focuses on the fabrication of HA by *S. zooepidemicus*, intending to employ statistical techniques to optimize the production circumstances.

Carbon supply, temperature, pH, and agitation rate were the most critical factors influencing production. RSM established on the CCD was an effective statistical method for determining the synergy between the four preferred criteria and accelerating hyaluronic acid production.

For the verification of the synergy between the determinants and responses, the data was examined utilizing the Minitab 16 application and analysis of variance (ANOVA).

3.5. Impacts of aeration and agitation rates on oxygen transfer coefficient

3.5.1. Fermentation medium composition

After optimizing the medium for HA production, the next step was to study the k_La rates. The following components (g/L) constituted the medium: sugarcane molasses (10% v/v), yeast extract, KH_2PO_4, 1.5 $Na_2HPO_4.12H_2O$, and 0.5 $MgSO_4.7H_2O$. The medium was autoclaved for 15 minutes at 121 °C.

The molasses was autoclaved separately, and once they reached room temperature, they were mixed with the remaining media aseptically to avoid caramelization. Molasses made from agricultural and industrial waste have enough carbon to serve as a cheap energy source for fermentation.

Without protein or fat, molasses is 75% carbohydrates and 22% water. Reducing sugars in molasses is roughly 17% overall (Awad El-Kareem, 2003). Molasses comprises of sugars glucose (12%), sucrose (29%), and fructose (13%) (Shukla et al., 2022b). The inoculum was prepared in a similar way as described in section 3.4.2.

3.5.2. Assessment in Bioreactor Systems

The pH was automatically kept at 6.8 throughout the fermentation process using HCl (2 M) and NaOH (2 M). A 37 ºC cultivation temperature was maintained. Aeration pressure and flow rate were set at 1.5 m^3/h and 0.1 MP, respectively.

A polarographic electrode was used to measure DO, which was then indicated as an O_2 saturation percentage. As a result, real-time data-gathering software may be used to monitor the values of OUR and k_La online.

The fermenting process lasted 36 hours. Every two hours, 5 mL of the sample was withdrawn to analyze the dry cell weight, sugar concentration, and product formation. Additionally, every four hours, 2 mL of the sample was taken to explore the formation of lactic acid (LA) as LA forms naturally with the production of HA.

To analyze the effects of oxygen on OUR, HA production, OTR, k_La, and rheological characteristics, four distinct cultures were examined at agitation rates of 150, 200, 250, and 300 rpm, respectively. Each experiment was performed in triplicates.

3.6. Kinetic model

3.6.1. Microbial growth

Equation (3) can potentially determine the biomass development rate.

$r_x = \frac{dx}{dt} = \mu X$ Equation (3)

Here, the growth rate is (h^{-1}). The Verhulset or logistic model is frequently utilized to examine the behavior of microbial growth. The growth in different fermentation processes has been well described using the Verhulset model (Glaser & Venus, 2017), as given in equation (4).

$r_x = \frac{dx}{dt} = \mu_m X \left(\frac{X_m - X}{X_m}\right)$ Equation (4)

The maximum biomass is Xm (gL^{-1}) (h^{-1}), and the maximum specific growth rate is μ_m. Including Eq. (4),

$X = \frac{X_0 X_m e^{\mu_m t}}{X_m - X_0 + X_0 e^{\mu_m t}}$ Equation (5)

wherein the initial biomass concentration is given as X_0 (gL^{-1}),

By considering the logarithm of the culture period, λ_x, (h), and the maximal growth rate, v_x ($gL^{-1}h^{-1}$), Vázquez JA et al. (Vázquez & Murado, 2008) have given equation (6) by simplifying equation (5)

$X = \frac{X_m}{1+\exp[2+\frac{4v_x}{X_m}(\lambda_x - t)]}$ Equation (6)

3.6.2. Consumption of substrates

The substrate consumed during microbial fermentation processes is used for product formation, biomass growth, and cell maintenance. Eq. (7) provides the equation for the mass balance of substrate used in batch fermentation.

$$-r_s = \frac{-ds}{dt} = \frac{1}{Y_{P/S}}\frac{dp}{dt} + \frac{1}{Y_{X/S}}\frac{dx}{dt} + m_s X \quad \text{Equation (7)}$$

Due to the low substrate flux for HA synthesis in the current investigation, the product term in Eq. (7) has been neglected (Don & Shoparwe, 2010; Vázquez et al., 2010), which will result in

$$\frac{ds}{dt} = -\frac{1}{Y_{X/S}}\frac{dx}{dt} - m_s X \quad \text{Equation (8)}$$

Where biomass yield coefficient (g/g) is given as $Y_{X/S}$, product yield coefficient (g/g) is shown as $Y_{P/S}$, and the maintenance coefficient (g/g/h) is given as m_s.

The final equation for substrate consumption as a function of time is shown below; after integrating equation (8) and introducing X (equation 6), equation 9 was obtained.

$$S = S_0 - \frac{1}{Y_{X/S}}\left[\frac{X_m}{1+e^{\left[2+\frac{4v_x}{X_m}(\lambda_x - t)\right]}} - X_0\right] - \left(\frac{m_s X_m^2}{4v_x}\right)\ln\left[\frac{X_0\left(e^{\frac{4v_x}{X_m}t} - 1\right) + X_m}{X_m}\right] \quad \text{Equation (9)}$$

Where the initial substrate concentration (g/L) is given as S_0.

3.6.3. Product Formation

The Leudeking-Piret equation has the potential to determine LA and HA production.

$$r_p = \frac{dp}{dt} = \frac{dx}{dt}\alpha + \beta x \quad \text{Equation (10)}$$

For non-growth-related and growth-related product development, respectively, the Leudeking-Piret constants are α and β.

The final equation for product production as a function of time is as follows: integrating equation (10) and replacing the X (equation 6):

$$HA = \left[\frac{\alpha_{HA}X_m}{1+e^{\left[2+\frac{4v_m}{X_m}(\lambda_x - t)\right]}} - \alpha_{HA}X_0\right] + \left(\frac{\beta_{HA}X_m^2}{4v_x}\right)\ln\left[\frac{X_0\left(e^{\frac{4v_x}{X_m}t} - 1\right) + X_m}{X_m}\right] \quad \text{Equation (11)}$$

$$LA = \left[\frac{\alpha_{LA}X_m}{1+e^{\left[2+\frac{4v_m}{X_m}(\lambda_x - t)\right]}} - \alpha_{LA}X_0\right] + \left(\frac{\beta_{LA}X_m^2}{4v_x}\right)\ln\left[\frac{X_0\left(e^{\frac{4v_x}{X_m}t} - 1\right) + X_m}{X_m}\right] \quad \text{Equation (12)}$$

Where α_{LA} and α_{HA} are the Leudeking-Piret constants (g/g) of LA and HA that are associated with growth, respectively, β_{LA} and β_{HA} are the non-growth associated Leudeking-Piret constants (g/g/h) of LA and HA.

3.6.4. OTR, OUR, and k_La values

The dynamic gassing-out method was also implemented during fermentation to calculate the k_La, OUR, and OTR (Garcia-Ochoa et al., 2000). The dissolved oxygen concentration is measured as the percentage of dissolved oxygen tension (DOT).

Mass balance could be used to generate an equation for variations in soluble oxygen in batch fermentation:

$$dC_0/dt = OTR - OUR = K_La.(C^* - C) - Qo_2.C_x \quad \text{Equation (13)}$$

where the volumetric OTR and OUR are represented by the variables k_La (C^* - C) and (Qo_2. C_x). The airflow was stopped at the intake (OTR = 0), and the DOT value dropped due to cellular respiration.

The OUR was then calculated as the slope of the curve (DOT vs. time). In line with Eq. (14),

$dC_0/dt = OUR = -(Qo_{2.}\ C_x)$ Equation (14)

The air inlet was restarted to increase the DOT to determine OTR, and the OTR value was calculated following Eq. (15),

$OTR = dC_0/dt + OUR$ Equation (15)

By monitoring the entire airflow, the oxygen concentration differential between the intake and outflow air, and the dissolved oxygen concentration, C_L, it is possible to calculate the overall volumetric oxygen mass transfer coefficient (K_La) in fermentation systems.

The following equation (16) can be used to plot K_La against time (Figure 3.2) (Zokaei-Kadijani et al., 2013)

$K_La = \frac{Fo_2^{in} - Fo_2^{out}(t)}{V(C^* - C_L)}$ Equation (16)

the molar flow rates recorded are FO_2in and FO_2out at the bioreactor intake and outlet, and the broth volume is C_L, giving V.

The oxygen concentration in the liquid phase. Considering the provided circumstances of temperature and pressure, the oxygen saturation or equilibrium concentration in the medium is denoted by the symbol C*.

Since the gas phase resistance can typically be omitted and the liquid side of the interface has the highest acceptable resistance to mass transfer, $k_L = k_L$, which means $K_La = k_La$, denotes the mass transport coefficient.

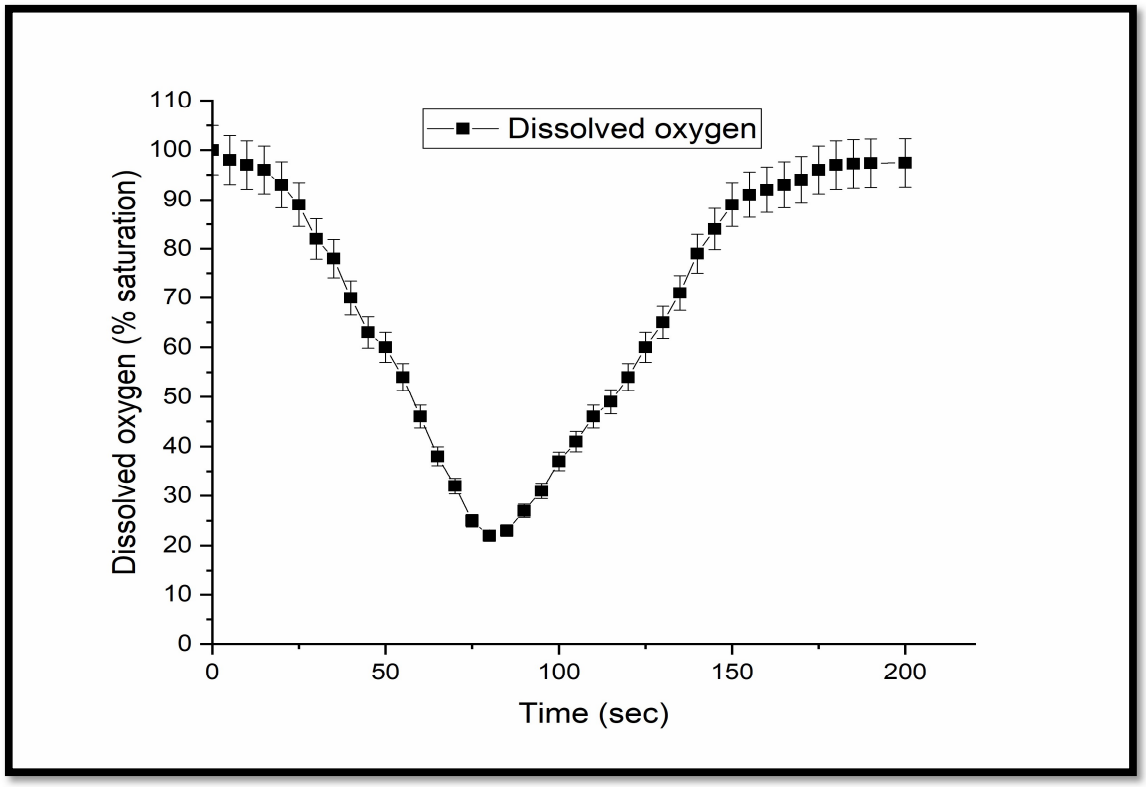

Figure 3.2. The experimental graph obtained during the gassing out technique for k_La determination

3.6.5. Rheological studies

The shear stress (τ, Pa) and shear rate (γ, s^{-1}) were displayed as the Y- and X-axis, respectively, in log form. The Ostwald-de Waele model of Eq. (17) explains the association between τ and γ;

$\tau = K(\gamma)^{\eta}$ Equation (17)

the η value represents the flow index, and the consistency index is given by the K value (mPa s or cp). The η number was utilized to determine whether the shear behavior of this biopolymer was shear thickening (η > 1) or thinning (η < 1).

3.7. Analytical methods

3.7.1. Biomass determination

The culture broth (1 mL) was removed from the culture every two hours and centrifuged (15 min at 8000 rpm). The retentate was washed out with 2 mL of 0.8% w/w saline solution after the supernatant was discarded.

The cell pellets were dehydrated in an oven at 50 ºC for 24 hours. The weight of the dried biomass was evaluated once it had been cooled to room temperature in the desiccator.

3.7.2. Total sugar estimation

Total sugar estimation was approximated using phenol sulfuric methodology (Masuko et al., 2005). A UV Spectrophotometer (Shimadzu, Japan) was used to measure the absorbance of the samples at 490 nm, and a standard curve was plotted (Figure 3.3).

3.7.3. Hyaluronic acid estimation

The sample was mixed with an equivalent amount of sodium dodecyl sulfate, 0.1% (v/v), centrifuged (10 minutes, 8000 rpm), and the supernatant was collected. The supernatant was separated utilizing four volumes of 100% ethanol, and HA was then precipitated by incubating the mixture at 4 °C for an hour.

It formed HA pellets after being centrifuged at 8000 rpm for 10 minutes. The cetyl trimethyl ammonium bromide method (CTM) was used to determine the amount of HA (Chen & Wang, 2009). A standard curve was plotted using standard HA (figure 3.4)

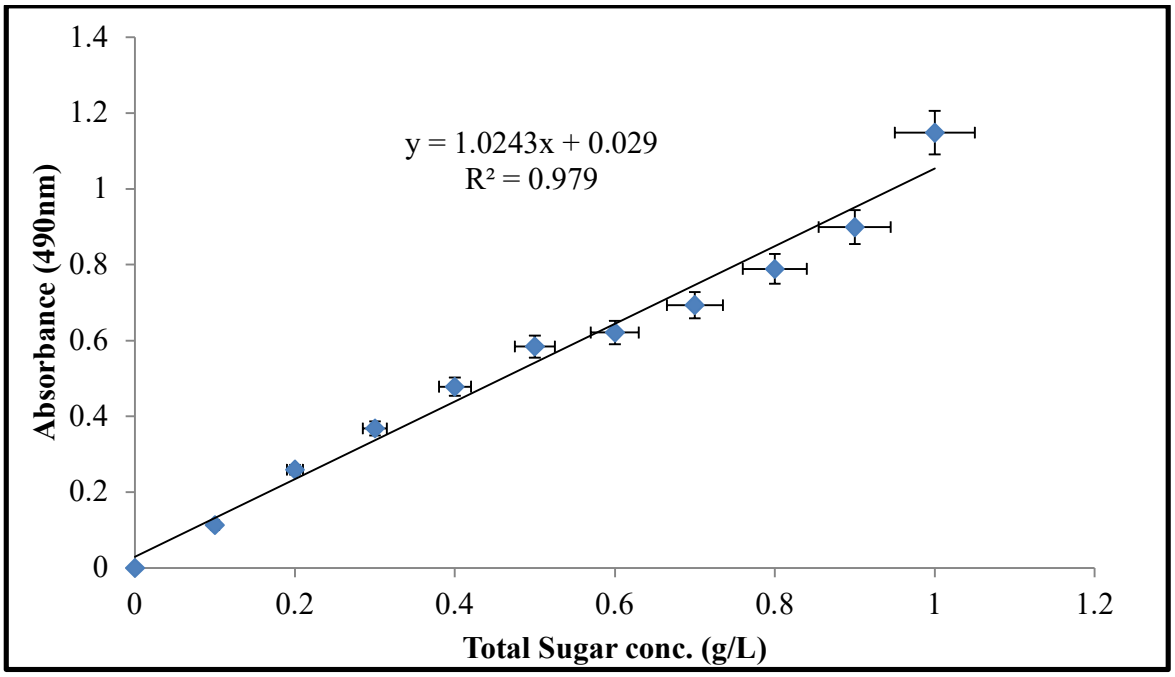

Figure 3.3. Total sugar concentration standard curve

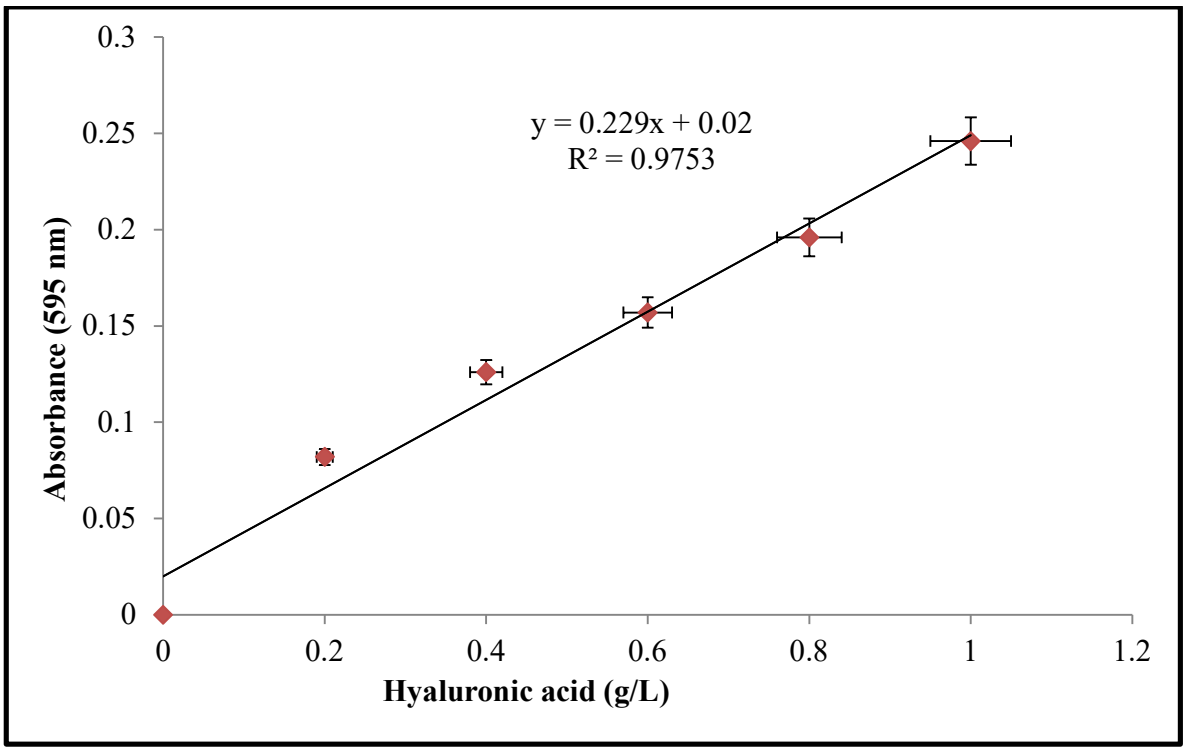

Figure 3.4. The hyaluronic acid standard curve

3.8. Optimization using artificial neural networking

Researchers introduced the uniform design (UD) method to provide statistics appropriate for real-world production. The UD approach has been effectively used in various optimization processes (Liang et al., 2001).

Artificial intelligence-based methodologies, counting artificial neural networks (ANN) and genetic algorithms (GA), are available as alternatives. ANNs have been effectively employed for media optimization and can imitate several elements of biological information processing (Singh et al., 2008; Singh et al., 2009). They offer an effective method for researching nonlinear issues.

ANNs are mathematical models representing the connections within experimental data through finite iterative computation, as opposed to regression equations that must be derived from a function of the experimental data.

ANNs can mimic the bioprocess and forecast the outcomes because of their higher modeling accuracy and improved generalization skills (Di Massimo et al., 1991; Schubert et al., 1994; Simutis & Lübbert, 1997; Vlassides et al., 2001). All nonlinear multivariate functions can be modeled with ANNs instead of standard statistical techniques, which can only do so for quadratic functions (Kramer, 1991; Walczak & Massart, 1996).

According to other reports, ANNs are frequently more precise than RSMs (Baş & Boyacı, 2007; Desai et al., 2008; Ilomuanya et al., 2020; Liu et al., 2009b). UDs typically feature patterns that are pretty representative and evenly spaced. Based on these high-quality patterns, with a lot less data than they are anticipated to require, ANNs are capable of producing equally accurate models.

3.8.1. Methods for predictive modeling and optimization

The Artificial Neural Network (ANN), a machine learning algorithm, incorporates estimating and simulation capabilities based on data inputs (Ali & Kamoun, 1993; Dayhoff & DeLeo, 2001; Yegnanarayana, 2009). Neurons in interconnected artificial neural networks can often determine values from inputs and respond to different circumstances.

As a result, ANNs are capable of pattern recognition and numerical prediction. Inferring a function from observation has been increasingly common in recent years, especially when the task or the data are too challenging for human brains to handle.

Several models employing general regression neural networks (GRNNs) and multilayered feed-forward neural networks (MLFNs) to enhance the fed-batch fermentation properties of HA were developed.

3.8.2. Multilayer feed-forward neural networks

The predominantly utilized neural networks are MLFNs taught using a back-propagation learning technique (Johansson et al., 1991; Smits et al., 1994; Svozil et al., 1997). These tackle many chemistry-related issues (Johansson et al., 1991). The synapses in an MLFN paradigm are arranged in layers, as illustrated in Figure 3.5.

The input layer is the top layer, the output layer is the bottom layer, and the in-between layers are considered to be the hidden ones. The mapping function Γ fundamentally allocates each neuron a subset $\Gamma(i) \subseteq V$ formed consisting of every progenitor of the defined neuron, which can be used to formalize the specification of the neurons.

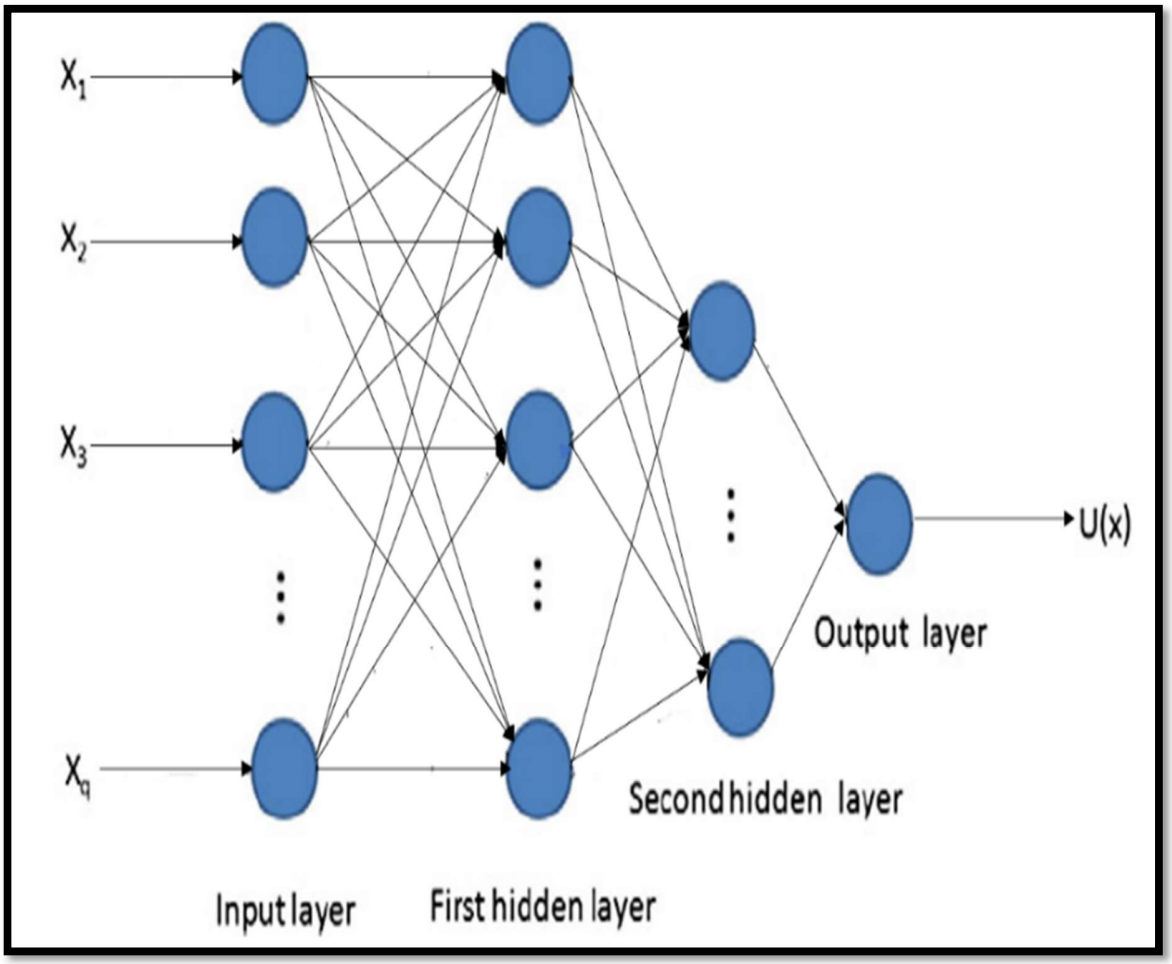

Figure 3.5. Multilayered feed-forward neural networks (MLFN) structure.

All the neurons that came before the specified neuron ί make up the subset Γ(ί)- 1 ⊆ V. The neurons in the layer above and below are all interconnected.

The threshold coefficient ϑί and the weight coefficient ω_{ij}, correspondingly, stand for the relationship seen between $ί^{th}$ and j^{th} neurons (Figure 3.6). The weight coefficient indicates how significant a particular neural network circuit is. Equations 18 and 19 are used to compute the output rebuttal of $ί^{th}$ neuron x^i.

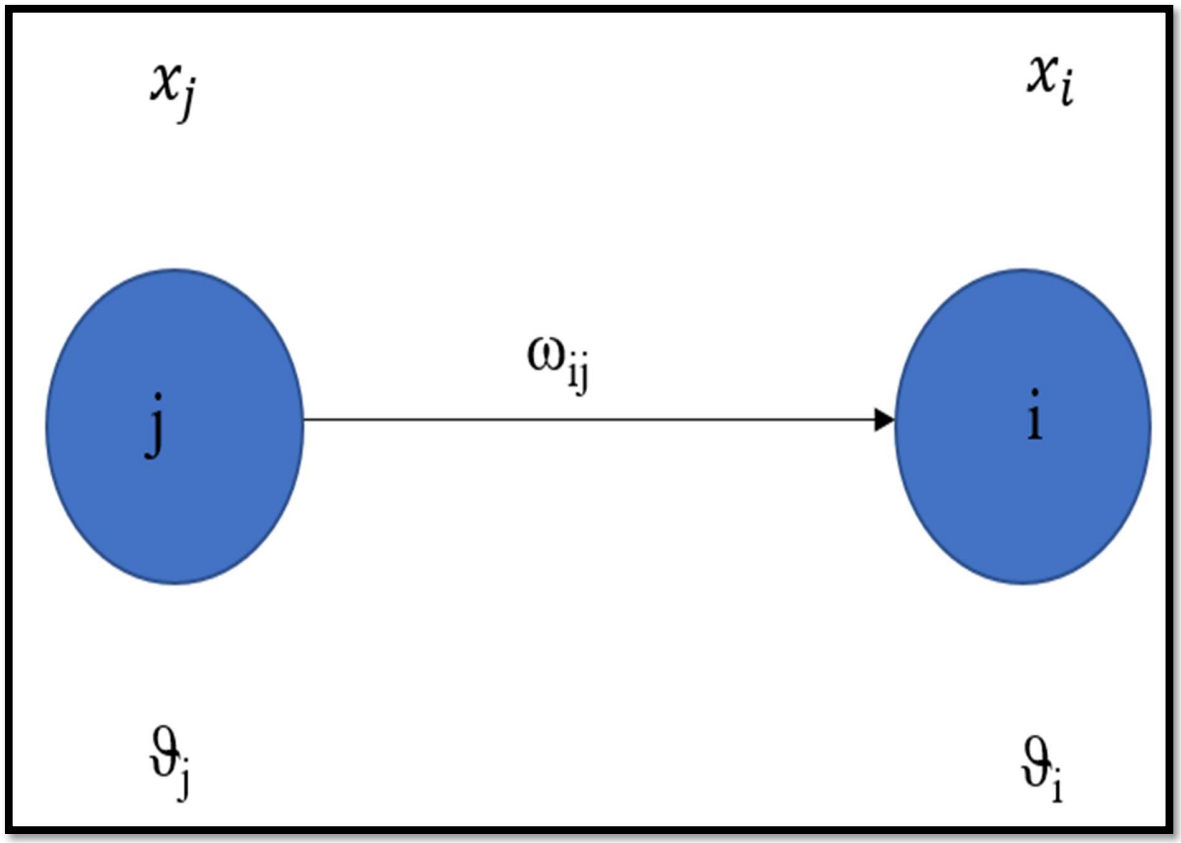

Figure 3.6. The connection between neurons i and j

These circumstances state that.

$x_i = f(\xi_i)$ Equation 18

$\xi_i = \vartheta_i + \sum_{j \in r_i^{-1}} \omega_{ij} x_j$ Equation 19

where ζ_i is the i^{th} neuron's potential and function $f(\zeta_i)$ is what is referred to as the transfer function (the summing in [Equation 19] transfers the signal to the i^{th} neuron by operating over all neurons j). It is feasible to interpret the threshold coefficient for $x_j = 1$ as a weight coefficient of said association with the functionally activated neuron j (so-called bias).

It is accurate for the transfer function.

$f(\zeta) = \frac{1}{1+\exp(-\zeta)}$ Equation 20

The weight coefficient ω_{ij} and threshold coefficient ϑ_i are adjusted during the supervised adaptation process to decrease the square root of the sum of the output value discrepancies that were computed and those that were required. The objective function E is minimized to achieve this.

$E = \sum_0 \frac{1}{2}(x_0 - \hat{x}_0)^2$ Equation 21

where summing is applied to all output neurons, and the vectors conjured up of the computed and obligatory exercise of the output neurons are x_0 and $\hat{x}_0$.

3.8.3. General regression neural network

Specht was the first to develop a General regression neural network (Specht, 2006). It performs effectively in three-dimensional modeling, pattern recognition, medical diagnosis, prediction, and chemical engineering (Baxt, 1991; Goulermas et al., 2007; Hoskins & Himmelblau, 1988; Kandirmaz et al., 2014; Khan et al., 2001; Li et al., 2014). In real applications, GRNN typically outperformed other neural networks in approximation (Kandirmaz et al., 2014).

Consistency, fast learning, and ideal regression with lots of data are the characteristics of the GRNN (Cheerla et al., 2018). Input, pattern, summation, and output are the four layers of a GRNN, as depicted in Figure 3.7 (Cheerla et al., 2018). The input layer maintains the corresponding input while passing the input vector x to the prediction phase. Neurons in the pattern layer serve as training data.

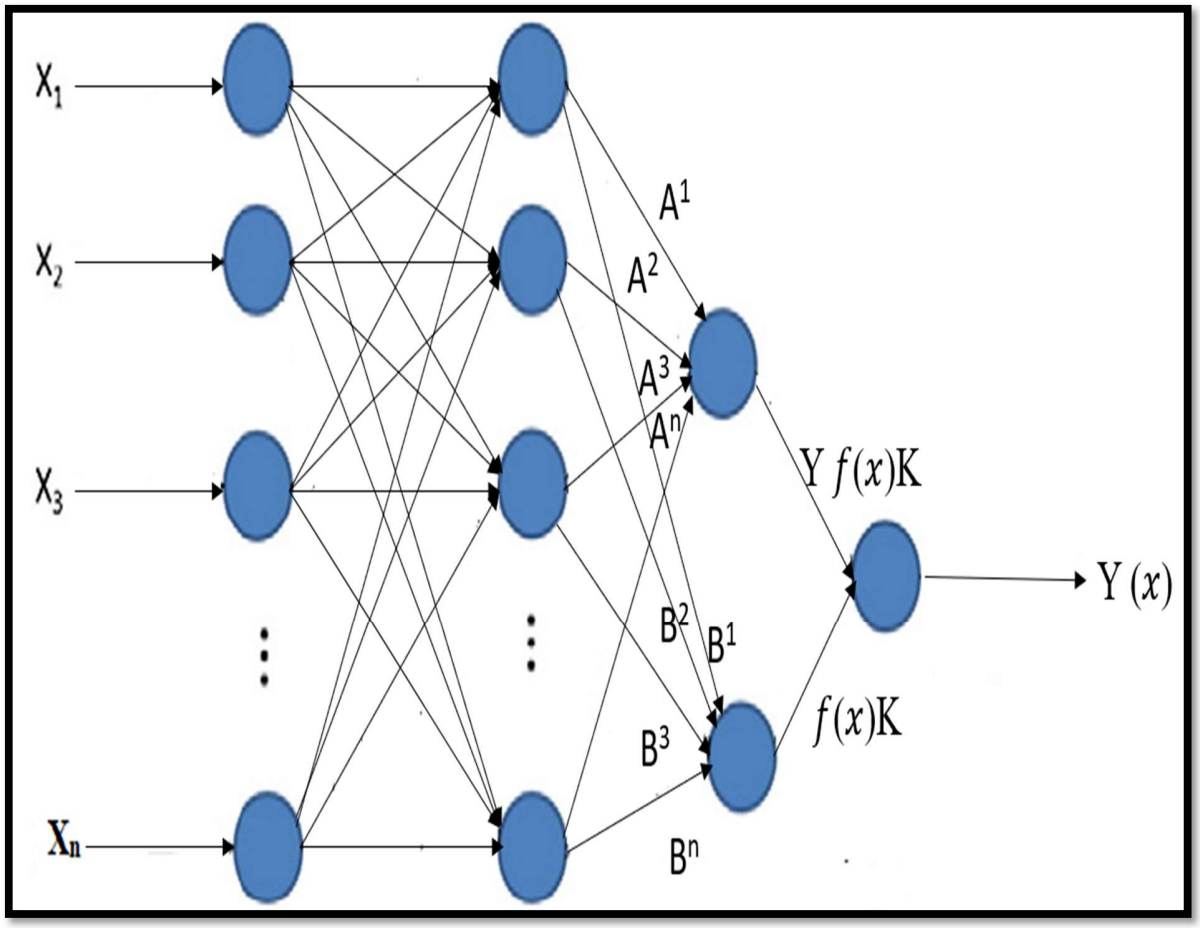

Figure 3.7. General regression neural networks (GRNNs) Structure

Equation 22 can be used to determine the weighted squared Euclidean distance in this layer.

$D_j = (x - x_j)^T - (x - x_j)$, [Equation 22]

The network's test inputs are first subtracted from the values of the neurons in the pattern layer. Additionally, subtractions using the exponential activation function will result in a squared or absolute total. The summation layer receives the outcome. As the outputs and weights of each pattern layer are added, the summation layer neurons compute the dot

product. The y values of the training data fed in the pattern layer are used to calculate the values of the weights, which are shown in Figure 3.7 as A and B.

Weighted outputs of the pattern layer are represented by $f(x)$K, where K refers to the Parzen window's constant. Y $f(x)$K is the multiplication of the outputs from the pattern layer and the training set. To determine the desired Y's estimation, as described in [Equations 23 and 24], f $f(x)$K divides Y $f(x)$K at the output layer.

$$Y(x) = \frac{\int_{-\infty}^{\infty} Yf(x,Y)\mathrm{dY}}{\int_{-\infty}^{\infty} Yf(x,Y)\mathrm{dY}}, \quad \text{Equation 23}$$

$$Y(x) = \frac{\sum_{j=1}^{p} y_j e[-\frac{D_j}{2\sigma^2}]}{\sum_{j}^{p} e[-\frac{D_j}{2\sigma^2}]} \quad \text{Equation 24}$$

3.8.4. SVM model

The primary foundation of the learning algorithm SVM is statistical learning theory (Deng et al., 2012). This approach has a high potential for global optimization to boost generalization based on the restricted knowledge of samples regarding models' sophistication and training capability.

A fundamental SVM principle for linear separable binary classification is the discovery of the best hyperplane, which has the most significant margin of separation between each specimen (Shen et al., 2012; Zhong et al., 2013).

The plane contributes to the model's capacity to anticipate the future while also assisting in lowering the classification mistakes that can occasionally arise.

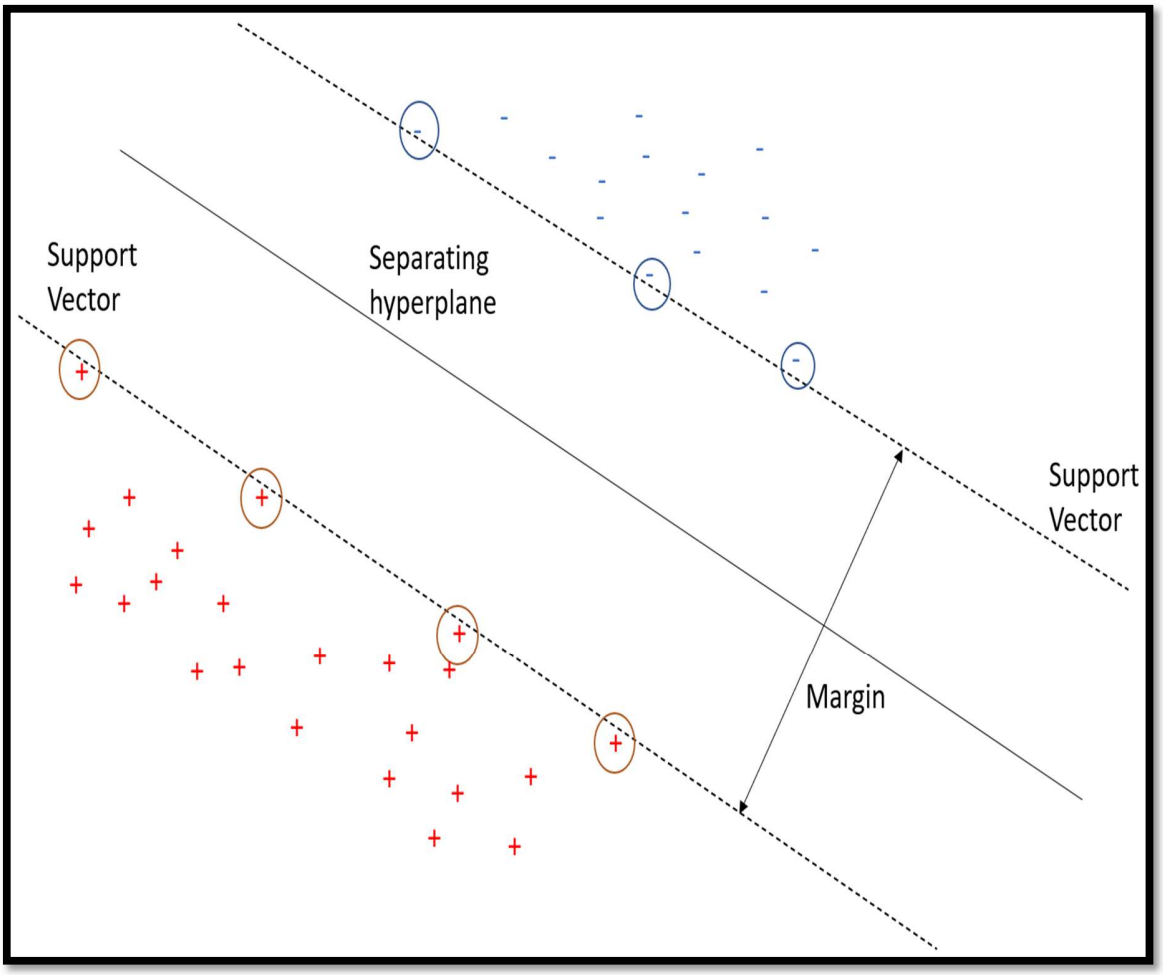

Figure 3.8. Support vectors specify where the ideal hyperplane should be.

The ideal hyperplane is shown in Figure 3.8, with "+" denoting type 1 samples and "-" denoting type -1 samples. Figure 3.9 illustrates the SVM's structural framework. Kernels are represented by the letter "K" (Kim et al., 2005). The figure shows that the SVM comprises a tiny subset taken from the training data by the appropriate procedure. Selecting optimal kernels and parameters is crucial to achieving prediction accuracy in classification.

However, the criteria cannot be chosen now as an established international standard is lacking. In most cases, comparing experimental results, learning from extensive calculations,

and using cross-validation provided by software packages assist us in partially resolving that issue (Fan et al., 2008; Guo & Liu, 2010).

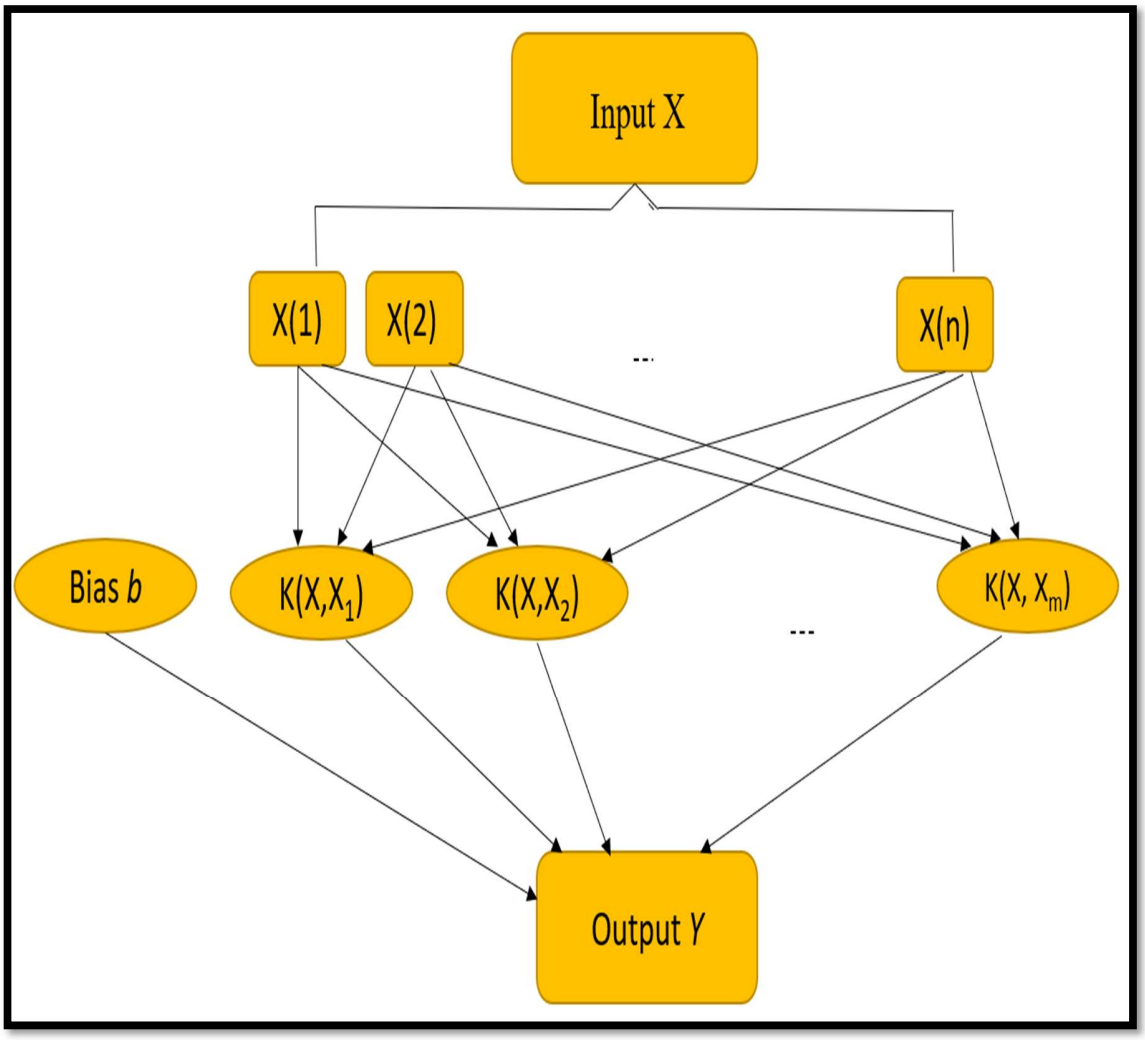

Figure 3.9. The support vector machine's primary structure.

3.9. Purification of hyaluronic acid

A sharp rise in the market for HA products produced via bacterial fermentation has occurred recently because of the immunological effects caused by HA derived from animals. To meet the stringent standards for HA use in medical products, the strains of bacteria and

purification procedures used for HA production are selected more based on quality than quantity.

Process intensification (PI) is necessary to reduce material and energy consumption and the environmental impact while providing greater flexibility in operation through innovative products and processes.

An effective process intensification requires the selection of appropriate membranes and modules in cell separation and product purification, as well as the provision of logical sequencing of operations.

The goal is to develop a purification process that can produce HA of a biomedical quality while being facile and economically viable. When purifying HA, eliminating the proteoglycan matrix's peptides and proteins is the biggest challenge. The finished product may contain these potentially allergenic proteins.

Final protein concentrations for clinically applicable preparations requiring injection should be in the range of 5–10 μg of protein per g of HA, and the standards for purity for non-injectable performances to 5–10 mg of protein per g of HA (perfusion, topical application, oral administration) (Murado et al., 2012).

3.9.1. Hyaluronic acid recovery and purification

The downstream procedure for microbial HA frequently entails alcohol precipitation, activated charcoal adsorption, silica gel adsorption, and diafiltration (Patil et al., 2011). The primary contaminants in microbially produced HA are proteins (Cavalcanti et al., 2020). A pre-purification step was performed to liberate the HA from the cellular membrane by adding

0.01% sodium dodecyl sulfate (SDS) in the fermentation medium to initiate the purification process.

SDS cultures were titrated after 15 min of adding 10% hexadecyltrimethylammonium bromide solution for floc formation. To solubilize this precipitate in 2 M $CaCl_2$, approximately one-tenth to one-twentieth of the initial present volume was added. In the end, the supernatant was collected after centrifuging the suspension.

Precipitation using organic solvents or quaternary salts has been employed extensively to remove proteins. Precipitation typically appears in the earliest stages of the HA purification procedures because of its efficiency in eliminating the majority of proteins and other impurities (Murado et al., 2012).

The HA produced during submerged fermentation was diluted with ethanol (3:2 v/v), kept for 2 h at -20 ºC, and centrifuged (7000 rpm, 30 min). The precipitate was treated with 1 M NaCl solution, and the salting out effect was studied at various pH ranges from 4 to 7.

Activated charcoal in the form of powder and granules was steam-activated before being dried at 105 ºC for 4 h. Granular activated charcoal was utilized immediately. In contrast, powdered activated charcoal was filtered through one sieved filter, accumulated, and dumped in hot water to eliminate air.

The primary purpose of using charcoal was to remove the unwanted color from the medium, which was present due to the use of molasses in the production process. The use of activated charcoal as a decolorization agent has been validated in several studies (Kumar, 2003).

HA (standard) solution containing 5, 50, 100, 200, and 500 mg/100 mL, respectively, was mixed with activated charcoal (0.5 g) and maintained at 37 °C and 150 rpm for an hour in a

beaker. Whatman no. 42 filter paper was used to filter the mixtures, and 50 mL of deionized water was used to wash away the filtering residue.

A 200 mL final volume was made from the filtrate and deionized water. Then, HA in the filtrate was detected by a UV spectrophotometer at 595 nm. Adsorption % and capacity were determined using the following formulas (Eq. 25 and Eq. 26):

$$Adsorption\ Capacity = \frac{HA\ in\ solution\ before\ adsorption - \quad in\ filtrate}{Weigh\ \ of\ activated\ charcoal} \quad \text{Equation 25}$$

$$Adsorption\ Percentage = \frac{HA\ in\ solution\ before\ adsorption \quad in\ filtrate}{HA\ in\ the\ solution\ before\ adsorption} \quad \text{Equation 26}$$

The fermented broth was treated with 1% active charcoal (150 rpm, 30 min) and centrifuged (8000 rpm, 30 min) at 4 ºC to obtain a clear solution.

Filter papers were placed at the bottom of a column of 1 g of HA-adsorbed activated charcoal loaded upwardly. Employing 50 mL of ethanol, ethanol/HCl (49:1), acetic ether, NaOH (0.5%, 1%, 1.5%, and 2.0%), and hot water (90 ºC), respectively, at 1 mL/min, desorption was carried out downwards, and the amount of HA in the elute was calculated.

The experiments were performed at room temperature, and since extreme pH may degrade HA, the pH was maintained at 7 for all the eluents.

A slightly polar neutral amber lite XAD-7 resins were utilized next for the protein adsorption process. The resins were adequately cleaned with deionized water for 30 min before use (to eliminate potential pollutants such as NaCl and Na_2CO_3) and acetone for 30 min to remove organic impurities (Kunin, 1977).

A constant amount of n-hexane was used to cleanse them, and they were dried at 70 °C and then placed into a hot air oven at 50 °C until they were required. The fermentation broth (500mL) was mixed with 1g of XAD-7.

It was necessary to add either 0.1 M NaOH or HCl to keep the pH of the solution at 6.8. The adsorption studies were conducted in a shaker at 25 °C. Filtration was used to separate the resins from the solutions after 30 min, and samples (5 mL) were then taken to determine the concentrations of proteins removed by Bradford assay.

With an MW cut-off of 300 kDa, a UF membrane cassette was used for the diafiltration process. The filtered broth underwent continuous mode diafiltration using deionized water as the diluent at room temperature. The cross-flow rate and transmembrane pressure were persistent at 40 mL/min and 1.5 bar, respectively.

After each diavolume, samples were taken for examination. Parameters like purity of HA and retention were calculated during the diafiltration process. 0.1 N sodium hydroxide was used for membrane washing and storing. The retentate was concentrated and vacuum-dried to obtain a white hyaluronate powder.

3.9.2. Protein and endotoxin determination

The Bradford test detected the peptides and protein concentration in the broth (Kruger, 2009). The 5 mL of Bradford reagent was added to the 1 mL sample, and then the sample was incubated at room temperature for 5 minutes with complete stirring.

The protein amount was determined using a standard diagram after measuring the absorbance at 595 nm. Optical density measurements at 260 nm determined the nucleic acid concentration.

The amount of residual endotoxin was determined using the kinetic chromogenic technique (Lonza, USA, Kinetic-QCL Chromogenic LAL (Limulus amebocyte lysate) test) (Choi et al., 2014) and after adding the LAL kinetic chromogenic reagent to the standard and test

solutions, then evaluated the transmittance of it at a wavelength of 405 nm (Choi et al., 2014).

The standards were diluted to 5, 0.5, 0.05, and 0.005 EU/mL using the LAL reagent water to produce two mL standard solutions (Lonza Co., USA). To reduce the impact of inhibitory factors, the sample solution was diluted as little as possible before being turned into the test solution. The LAL reagent was made by mixing the LAL kinetic chromogenic reagent and its reagent water.

3.10. Hyaluronic acid characterizations

In addition to performing HPLC, FTIR, SEM, XRD, and NMR on the purified HA, its antioxidant properties were determined.

3.10.1. High-performance liquid chromatography

Hyaluronic acid produced by fermentation was sampled and evaluated by working on high-performance liquid chromatography (Shimadzu, Japan). The collected specimen was thinned in 0.1 N HCl, refined through 0.2 µm filters, and examined using the C_{18} column (Harmita et al., 2020).

The mobile phase used was water and methanol at a ratio of 96:4, and the solution was degassed for 30 minutes. The flow rate was confirmed at 1 mL per minute at a temperature of 25ºC, the output was unearthed at 280 nm wavelength using a UV visible detector, and the sample volume injected was 10 µl.

The standard hyaluronic acid solution was prepared to dissolve 200 mg of HPLC-grade authentic hyaluronic acid (HIMEDIA) in 100 mL of 0.1 N HCl and diluted to 10 µg per mL concentration (Harmita et al., 2020).

3.10.2. Mass spectroscopy

For the probe of HA and its derivatives, MS is significant. It has a high sensitivity for detecting HA. It can distinguish HA from other GAG structures, depict MW directly, improve SEC's skills for determining MW distribution, and even show HA geographical distribution.

Electrospray ionization methods for HA analysis and matrix-assisted laser desorption/ionization are the most extensively utilized ionization methods. Due to the absence of labile residues (such as fucose, sialic acid, or sulfate) in HA, rapid atom bombardment without in-source fragmentation was used to ionize the produced disaccharides under harsher circumstances. (Okuda et al., 1994).

The X500 QTOF Mass Spectrometer (SCIEX) was used to perform the ESI-MS observations. Spectra were obtained in negative ionization mode at a scan speed of 1 second from m/z 200 to 1000.

3.10.3. Fourier Transform- Infrared Spectroscopy

Purified HA was mixed with dry KBr powder to make pellets, then pressed under vacuum for 20 min at a 50–100 kg cm^{-2} pressure. The peaks of these pellets were in the range of 500–3500 cm^{-1} as they passed to the FTIR spectroscopic instrument for spectral analysis.

3.10.4. Scanning electron microscope

Scanning electron microscopy (SEM) (Nova Nano SEM 450 Scanning Electron Microscope) was performed at 15 kV to visualize the morphological characteristics of hyaluronic acid. HA cross-sections were coated with gold before analyzing and recording the data.

3.10.5. X-ray diffraction

X-ray diffraction examinations to characterize the microbial HA using a Rigaku SmartLab 9 kW Powder type with a Cu tube (K" radiation). The results were obtained between 0 ºC and 40 ºC.

3.10.6. Proton nuclear magnetic resonance

The structure of the hyaluronic acid was determined using a 300 MHz ^{1}H-NMR AVH D 500 AVANCE III HD 500 MHz OneBay NMR Spectrometer**.** Hyaluronic acid (10 mg) was dissolved in 350 µL D_2O.

3.10.7. Thermogravimetric analysis

The thermal stability of microbial HA and sodium hyaluronate samples was tested using an M/s Shimadzu (TGA-50) (Shimadzu, Japan). The analysis settings included a heating rate of 5 ºC/min, a 30-800 ºC temperature range, and a 50 mL/min flow rate for the nitrogen atmosphere.

3.10.8. Antioxidant assay

The phosphomolybdenum methodology (Kumaran & Karunakaran, 2007) was utilized to determine the sample's overall antioxidant capacity. As part of the experiment, samples (100 µL) were placed in tubes with 700 µL of distilled water, sodium phosphate (100 µL, 280 mM), and 100 µL of ammonium molybdate (40 mM).

A 90-minute incubation at 100 ºC followed by an analysis of absorbance at 695 nm followed. Concentrations of ascorbic acid (20 mg/mL to 300 mg/mL) were used to create a standard curve for converting the results to grams of ascorbic acid equivalent per gram of sample (g AAE/g).

Using Galinari *et al.*'s method, the sample was tested for its ability to chelate iron ions (Galinari et al., 2018). Incubation at 37 ºC for 10 minutes was carried out with sample (910

µL), ferrozine (60 µL, 5 mM), and ferrous chloride (30 µL, 2 mM). An absorbance measurement was performed at 562 nm.

An assessment of the sample's reduction potential was conducted by Wang *et al.* defined method (Wang et al., 2008). A total of each sample (200 µL) was treated with potassium ferricyanide (100 µL) for 20 minutes at 50 ºC, followed by ferric chloride (20 µL), 10% trichloroacetic acid (180 µL), and phosphate buffer (1.5 µL, 200 mM, pH 6.6) and per 0.1 g/L of ascorbic acid, calculated the reducing power using the absorbance at 700 nm.

Each sample (40 µL) was first dissolved in a DPPH solution to assess the sample's capacity to scavenge DPPH radicals (200 µL, 0.1 mM in ethanol) (Nóbrega et al., 2015). A microplate reader from BMG LABTECH read the results after 25 minutes of incubation.

According to Smirnoff and Cumbes, a test was run for the sample's ability to neutralize hydroxyl radicals (Smirnoff & Cumbes, 1989). 50 µL of each sample was combined with 10 mM ferrous sulfate heptahydrate, phosphate buffer (750 µL, 150 mM, pH 7.4), sodium salicylate (2 mM), and 10 mM EDTA. The mixture also contained hydrogen peroxide (200 µL, 30%). An incubation period of 60 minutes at 37 ºC was followed by a reading of the results at 510 nm.

To test each sample's ability to scavenge superoxide radicals, each sample (200 µL) was combined with phosphate buffer (200 µL, 50 mM, pH 7.4), EDTA (200 µL, 0.5 mM), methionine (200 µL, 65 mM), NBT (200 µL, 0.375 mM), and riboflavin (200 µL, 0.5 mM). After 15 minutes of fluorescent light incubation, the mixture was read against a blank to determine the absorbance at 560 nm (Dasgupta & De, 2007).

3.11. Hyaluronic acid as an antibacterial agent

An attractive candidate is a molecule with antibacterial and antioxidant activity to observe the antibacterial properties of hyaluronic acid. New antibacterial agents that target tyrosyl-tRNA synthetase can be developed or discovered (Xiao et al., 2011). In addition to catalyzing amino acid binding to their respective tRNAs, it belongs to the aaRSs (aminoacyl-tRNA synthetases) family; due to the critical role that aaRSs play in protein synthesis, inhibition of aaRSs inhibits cell growth.

A second target enzyme is Topoisomerase DNA gyrase II. Cell survival depends on DNA topoisomerases, enzymes that affect DNA topology. Type II topoisomerase DNA gyrase forms negative supercoils using ATP. Higher eukaryotes do not possess it, making it a good target for antibacterial drugs (Gibson et al., 2019). Considering this, hyaluronic acid's antibacterial properties can be evaluated.

Our study aimed to uncover how hyaluronic acid reacts with the targeted molecules. On Gram-negative and Gram-positive bacteria, hyaluronic acid was investigated for antibacterial properties. Computational analysis was used to explain better the processes of interaction of tyrosyl-tRNA synthetase and topoisomerase II DNA gyrase from *S. aureus* and *E. coli*. Ampicillin was taken as a reference standard antibiotic for our docking studies.

3.11.1. Computational studies

3.11.1.1. Preparation of protein and ligand for docking-

Under the aegis of the Protein Data Bank (PDB), the structures of tyrosyl-tRNA synthetase from *S. aureus* (PDB ID:1JIL) and *E. coli* (PDB ID:2YXN), as well as topoisomerase II DNA gyrase from *S. aureus* (PDB ID:5CDP) and *E. coli* (PDB ID:6RKS) were determined

(Berman et al., 2000). The SWISS PDB Viewer was utilized to minimize the energy of proteins after the final modeled structures (Guex & Peitsch, 1997).

The PyMOL visualizing tool was also used to check for any missing residues (heteroatoms or ligands) or water molecules in the model proteins. Chimera 1.13 prefabricated the docking protein (Pettersen et al., 2004). Gasteiger charges and hydrogens were added to the proteins and changed from SDF to PDB structure format.

The 3D structures of the ligands in the SDF format were obtained using the PubChem databases. Energy minimization of Ligands (hyaluronic acid and ampicillin) was performed using chimera1.13 (Pettersen et al., 2004). Subsequently, solvents were removed, created rotatable bonds, and the ligands were torched.

3.11.1.2. Docking Studies

AutoDock tools were employed to perform a molecular screening for all ligands utilizing MGLTools v. 1.5.6 and Raccoon (Morris et al., 2009). The ligands were kept flexible during docking, whereas the protein remained rigid.

Based on the information in the configuration files and the potential ligand-binding sites on the various enzymes, docking, and grid parameters were generated with the AutoDock and AutoGrid tools of the AutoDock4 platform. The grid boxes were selected one at a time to cover portions of the desired amino acids.

AUTODOCK4 was used to perform docking using the Lamarckian Genetic Algorithm (LGA) (Goodsell et al., 1996). It is significantly better than other search or simulation

algorithms offered by AUTODOCK. Based on the definitions of five terms in the literature, the AMBER force field is used as an algorithm (Venkatesan et al., 2010).

Using AUTODOCK4, the docked conformations were validated and analyzed, and conformations with the minimum binding energies for multiple interactions were examined.

3.11.1.3. Molecular dynamic simulation studies

After our molecular docking, molecular dynamics and simulation studies were used using apoproteins and protein-ligand complexes. Hyaluronic acid with various proteins was simulated. GROMACS 2018.8 was employed for our simulation studies.

Using PRODRG server v. 2.5, the GROMOS force field generated parameters and topological data for our compounds (Borkotoky & Banerjee, 2021; Van Aalten et al., 1996). The apoprotein and ligand complexes were solvated in a 1.2 nm cubic box using the GROMOS 54a7 (Abraham et al., 2015) force field and SPC/E water molecules.

In the ionization procedure, Na^+ and Cl^- ions neutralized the charge on the systems. The steepest descent technique was used for all plans with a 1000 kJ/mol tolerance for the energy minimization phase. A maximum of 50,000 steps was specified for energy minimization for all systems. The value established for long-range and short-range interactions, according to the PME technique, is 1.2 nm.

A 1ns NVT and NPT equilibration step was performed with fixed particle counts, volume, temperature, and energy minimization. Using the Berendsen thermostat (Borkotoky & Banerjee, 2021; Bussi et al., 2007), at 300 K, NVT equilibration with 0.002 fs time steps were performed.

The long-range interactions were conducted using the Particle Mesh Ewald (PME) technique, with a cutoff value of 1.2nm and Fourier spacing of 0.16nm (Hess et al., 1997).

Our NPT equilibration was performed at a given temperature, pressure, and number of particles. With a time constant of 2 fs, a pressure of 1.0 atm, and isothermal compressibility of 4.5 e^{-5} bar, Berendsen isotropic pressure coupling was established.

After the equilibration stages, a leap-frog integrator was used to simulate all systems for 50 ns with a dt of 2 fs (Borkotoky & Banerjee, 2021). GROMACS' basic instructions were used for all of the analyses.

For stretching all of the link lengths stated before (DeLano, 2002; Genheden & Ryde, 2015; Musyoka et al., 2016), the LINCS algorithm (Hess et al., 1997) was utilized (Kundu & Dubey, 2021; Kundu et al., 2021; Pande et al., 2022).

3.11.1.4. MM/PBSA free energy analysis

Using the MM/PBSA tool, our protein-ligand complexes' total free binding energy was determined, and the binding mode was selected using the GROMACS environment's gmx mmpbsa and pbsa.mdp scripts.

To save time, the free energy analysis was done in the last 20 nanoseconds of the experiment. Solutes and solvents have two and eighty dielectric constants, respectively (Genheden & Ryde, 2015; Musyoka et al., 2016).

3.11.1.5. Visual Analysis

In each example, the ligand's lowest energy conformation was chosen. PyMol-2.3.0 (DeLano, 2002) and Discovery Studio Visualizer (Dassault Systemes, BIOVIA, San Diego,

CA, USA(Biovia, 2017)) were used to analyze various interactions and generate 2D diagrams of the interaction patterns. Any hydrophobic interactions were validated using the PLIP server (Salentin et al., 2015), and LigPlot + was used to generate 2D diagrams (Laskowski & Swindells, 2011).